

Application of EXAFS spectroscopy to the study of abiotic redox processes in soils and sediments

A. Manceau

Environmental Geochemistry Group, University of Grenoble and CNRS, France

The past decade has witnessed explosive development in the application of non-invasive spectroscopic techniques, and specifically of synchrotron-based EXAFS spectroscopy, to determine the local structure of poorly-crystallized solids, the crystal chemistry of substituted elements, and the sorption mechanism of metals in contact with the major constituents of soils and sediments (clays, Fe and Mn oxides, phosphates, carbonates). Relatively few structural studies have been conducted on redox systems and, consequently, the nature of mineral transformations at the oxic-anoxic boundary so that the molecular-level mechanism of surface-induced redox reactions of trace elements are lacking. The capacity of EXAFS to determine the oxidation state and the structural environment of redox sensitive elements like Fe, Mn, Co and Cr will be illustrated with four case studies.

Structural transformation of Mn(IV) to Mn(II) in eutrophic lakes

The first example will concern the mineralogical transformation of poorly crystallized manganese minerals at the oxic/anoxic boundary during the cycling of manganese in the eutrophic Lake Sempach (Switzerland). Manganese oxide formed in the water column was identified as H-birnessite (Fig. 1) offering a large amount of vacancies in the octahedral layer for cation sorption. EXAFS spectroscopy revealed reduced manganese in the top 2 mm of the sediment indicating that the reduction of birnessite must occur at similar rates as the sedimentation, which is $2.5 \text{ mmol m}^{-2} \text{ d}^{-1}$ during summer. In the sediment, manganese is associated with authigenic $(\text{Ca}, \text{Mn})\text{CO}_3$ and $(\text{Fe}, \text{Mn})_3(\text{PO}_4)_2 \cdot 8\text{H}_2\text{O}$ particles. The relative amount of Mn in these two phases was quantitatively determined by EXAFS, yielding 55–60% manganese incorporated in carbonate and 40–45% manganese in phosphate particles. The average concentration of manganese amounts to 23 mol % in carbonate particles and 16 mol % in phosphate, thus indicating

that the proportion of phosphate and carbonate particles in the sediment is equivalent. With respect to the solid solutions, $(\text{Ca}, \text{Mn})\text{CO}_3$ and $(\text{Fe}, \text{Mn})_3(\text{PO}_4)_2 \cdot \text{H}_2\text{O}$, the porewater remains oversaturated from spring until autumn. Thus, dissolution of these phases is very unlikely. The remobilisation of manganese from the sediment into the deep water is therefore thought to be governed by other processes such as adsorption and desorption of Mn(II) on calcite surfaces.

Structural mechanism of Co(II) to Co(III) oxidation by the phyllo-manganate, birnessite

The geochemistry of cobalt at the Earth's surface is tightly associated with that of Mn oxides. Field evidences for this association are many and have been described on the sea-floor, in soils and in lateritic zones, where cobalt is always found precipitated with Mn-rich nodules, layers or crusts. The geochemical association of cobalt and manganese results from the oxidation of highly soluble Co(II) to weakly soluble Co(III), coupled with the reduction of Mn(IV)/Mn(III) to Mn(II). The molecular mechanism of the Co immobilization–birnessite dissolution process was investigated ex-situ and *in situ* (time-resolved) by EXAFS spectroscopy. Time-resolved experiments were realized with a stopped-flow instrument mounted on a dispersive spectrometer. With this set-up it is feasible to follow chemical reactions with half lives in the ms to s time range.

Two oxidation mechanisms were identified. In the first one, Co(II) sorbs above/below a vacant site (\square_1) of the Mn phyllo-manganate layer by sharing triple-corners with MnO_6 octahedra (Fig. 2, step 1). It is then oxidized by nearest \square_1 , and the resulting Co^{III} species fills in the \square_1 position while the reduced manganese migrate to the interlayer or in solution creating a new vacant site (\square_2) (Fig. 2, step 2). This reaction can be written: $\text{Co}^{\text{II}}_{\text{solution}} + \square_1 + \text{Mn}^{\text{III}}_{\text{layer}} \rightarrow \text{Co}^{\text{III}}_{\text{interlayer}} + \square_1 + \text{Mn}^{\text{II}}_{\text{layer}} \rightarrow \text{Co}^{\text{III}}_{\text{interlayer}} + \square_1 + \text{Mn}^{\text{II}}_{\text{layer}} \rightarrow \text{Co}^{\text{III}}_{\text{layer}} + \square_2 + \text{Mn}^{\text{II}}_{\text{sol/inter}}$. This mechanism

may replicate, since the density of vacancies remains constant, resulting at relatively high Co concentration to $\text{Co}_{\text{layer}}^{\text{III}}/\text{Mn}_{\text{layer}}^{\text{IV}}$ -rich domains. The second mechanism involves the replacement of $\text{Mn}_{\text{interlayer}}^{\text{III}}$ by $\text{Co}_{\text{interlayer}}^{\text{III}}$, and is eventually followed by the lattice migration of $\text{Co}_{\text{interlayer}}^{\text{III}}$, depending on the chemical composition of nearby layer octahedra (avoidance of $\text{Mn}_{\text{layer}}^{\text{III}}\text{-Co}_{\text{layer}}^{\text{III}}\text{-Mn}_{\text{layer}}^{\text{III}}$ sequences) (Fig. 3). This second mechanism can be schematically written: $\text{Co}_{\text{solution}}^{\text{II}} + \text{Mn}_{\text{interlayer}}^{\text{III}} + \square \rightarrow \text{Mn}_{\text{solution}}^{\text{II}} + \text{Co}_{\text{interlayer}}^{\text{III}} + \square \rightarrow \text{Mn}_{\text{solution}}^{\text{III}} + \text{Co}_{\text{layer}}^{\text{III}}$, the last step being conditional. In contrast to the first one, mechanism two results in a decrease of the density of vacant reactive sites.

The confrontation of these structural data, obtained on a model system, to those obtained for natural Co-containing Mn oxides (asbolane, lithiophorite) indicated that the two structural mechanisms explored in the laboratory satisfactory accounts for observations made on natural samples.

Structural mechanism of Cr(III) to Cr(VI) oxidation by the phyllo-manganate, birnessite

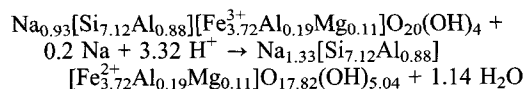
In aqueous media, Cr(III) can be oxidized to Cr(VI) by dissolved O_2 , and Mn(III) - Mn(IV) oxides. But for kinetics reasons, the oxidation of trivalent chromium is controlled by Mn oxides: The oxidation rate is speeded by several orders at their surface compared to the homogeneous oxidation. Kinetics studies of the oxidation process have identified Mn as the oxidizing agent. These studies have shown that the oxidation rate is independent of solution parameters such as pH, P_{O_2} , and ionic strength, but is proportional to the suspension concentration in solid. Whereas a surface controlled oxidation mechanism was demonstrated that way, uncertainties remained relative to the type of surface complex involved in the electron transfer reaction step. EXAFS and XANES have been used to determine the molecular mechanism of this surface catalyzed oxidation at the birnessite / solution interface. The oxidation process can be mechanistically depicted as follows: i) Free Cr(III) aqua ions diffuse towards Mn vacancies of the birnessite structure, as did cobalt in the previous example (Fig. 2); ii) the coupled Cr(III) oxidation/Mn reduction takes place; iii) Cr(VI) and Mn(II) ions are released in the solution, probably through the formation of an intermediate outer-sphere complex. This study provided the first evidence of a *double solid-state diffusion*, first towards, and then backwards from the sorbent. This mechanism is rendered feasible owing to a steric fit

between active sites (i.e. vacancies) of the sorbent and sorbate ions as both Mn(III/IV) and Cr(III) ions have similar ionic radii. In a certain sense, the vacant octahedral cages of birnessite act as a molecular sieve for Cr(III) free ions as polynuclear Cr(III) species are too large to enter reactive sites.

Structural mechanism of Fe(III) to Fe(II) reduction in the smectite, nontronite

The reduction of Fe(III) to Fe(II) is known to profoundly change the physical and chemical properties of clays including their cation exchange capacity, specific surface area, swelling behaviour, and ability to fix interlayer cations. Little is known about the structural mechanism of this redox transformation even though it is of key importance to the understanding of a number of environmental processes and to the deliberate modification of clay properties.

The structure of Garfield nontronite in the oxidized and reduced state was investigated by X-ray diffraction (XRD), polarized EXAFS (P-EXAFS), and texture analysis. XRD showed that oxidized Garfield is trans-vacant, whereas $24 \pm 5\%$ of total iron fill trans-octahedral sites in the reduced Garfield. The in-plane and out-of-plane local structure around Fe atoms was probed by angular P-EXAFS measurements on highly oriented self-supporting films. The dispersion of c^* axis around the film plane of individual crystallites was 20° FWHM for oxidized and 25° FWHM for the reduced sample. These narrow orientation distributions allowed us to treat the self-supporting films as single crystals during the quantitative analysis of P-EXAFS spectra. Iron(II) atoms were found to form small trioctahedral clusters separated by empty octahedra. The excess of negative layer charge resulting from the Fe reduction is partly compensated by the sorption of Na and H^+ from solution. Na occupies interlayer sites whereas H^+ lowers the negative layer charge by protonating structural OH^- groups of empty octahedra in the border of Fe(II)-rich domains, converting them into water molecules, and probably also by hydroxylating external oxygens. The average chemical reaction corresponding to this transformation can be written:



This mechanism provides a rationale to explain quantitatively a number of physico-chemical characteristics of reduced smectites.